AD-A161 922 PARTICLE DISTRIBUTIONS AND LASER-PARTICLE INTERACTIONS 1/1
IN AN RF DISCHARGE OF SILANE(U) NORTHWESTERN UNIV
EVANSTON IL DEPT OF CHEMISTRY K G SPEARS ET AL.
UNCLASSIFIED 20 NOV 85 TR-9 N00014-79-C-0622 F/G 20/9 NL

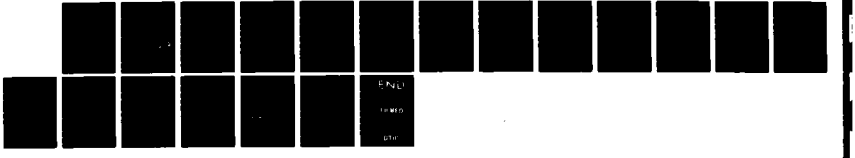

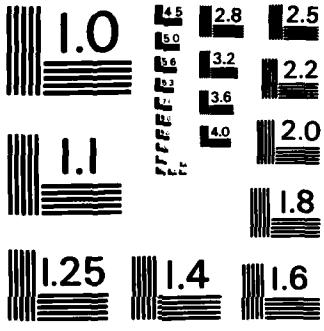

(12)

SECURITY CLASSIFICATION OF THIS PAGE (When Data Entered)

REPORT DOCUMENTATION PAGE

READ INSTRUCTIONS BEFORE COMPLETING FORM

1. REPORT NUMBER: Technical Report No. 9	2. GOVT ACCESSION NO.: AD-A161 922
3. RECIPIENT'S CATALOG NUMBER	
4. TITLE (and Subtitle): Particle Distributions and Laser-Particle Interactions in an RF Discharge of Silane	5. TYPE OF REPORT & PERIOD COVERED: Interim
	6. PERFORMING ORG. REPORT NUMBER
7. AUTHOR(s): Kenneth G. Spears, Timothy J. Robinson and Richard M. Roth	8. CONTRACT OR GRANT NUMBER(s): N00014-79-0622
9. PERFORMING ORGANIZATION NAME AND ADDRESS: Northwestern University, Department of Chemistry	10. PROGRAM ELEMENT, PROJECT, TASK AREA & WORK UNIT NUMBERS: NR 056-729
11. CONTROLLING OFFICE NAME AND ADDRESS: Office of Naval Research, Chemistry Program Code 472, Arlington, Virginia 22217	12. REPORT DATE: 11/20/1985
	13. NUMBER OF PAGES: 33
14. MONITORING AGENCY NAME & ADDRESS (if different from Controlling Office): ONR, Chicago, 536 South Clark Street, Chicago, Illinois 60605	15. SECURITY CLASS. (of this report): Unclassified
	15a. DECLASSIFICATION/DOWNGRADING SCHEDULE

16. DISTRIBUTION STATEMENT (of this Report)

Distribution of this document has been approved for public release and sale; its distribution is unlimited.

17. DISTRIBUTION STATEMENT (of the abstract entered in Block 20, if different from Report)

DTIC ELECTE DEC 04 1985 S D E

18. SUPPLEMENTARY NOTES

To be published in IEEE Transactions in Plasma Science February 1986

19. KEY WORDS (Continue on reverse side if necessary and identify by block number)

rf discharge; silane; plasma chemistry; particles; silicon atom; laser light scattering; laser-induced fluorescence.

20. ABSTRACT (Continue on reverse side if necessary and identify by block number)

A capacitively coupled, RF discharge of silane in argon was studied to determine particle distributions by light scattering and particle photophysics. Ultraviolet lasers cause silicon atom formation in both ground and excited states. Atoms were not formed with 354 or 532 nm excitation, but the discharge chemistry was affected by 354 nm excitation.

DD FORM 1 JAN 73 1473 EDITION OF 1 NOV 65 IS OBSOLETE S/N 0102-014-6601

SECURITY CLASSIFICATION OF THIS PAGE (When Data Entered)

85 12 2 006

AD-A161 922

DTIC FILE COPY

Particle Distributions and Laser-Particle Interactions in an RF Discharge of Silane

Kenneth G. Spears,[a] Timothy J. Robinson and Richard M. Roth[b]

Northwestern University

Department of Chemistry

Evanston, IL 60201

ABSTRACT

We report laser diagnostic studies of capacitively coupled, rf discharges containing 0.05-0.45% silane in argon. We probed positions between the plane parallel electrodes by pulsed laser light scattering at several wavelengths. These spatial scans had a resolution of 0.25 mm and they showed unusual particle distributions which varied with silane mole fraction and gas flow rates. Particle nucleation and growth kinetics were very well demonstrated over this range of discharge parameters. We also studied particle photophysics and demonstrated that ultraviolet pulsed lasers (251.4 and 266 nm) can form silicon atoms from laser-particle interactions. Atoms were formed in both ground and excited states with a concentration that depended linearly on laser energy. However, atoms were not formed by 354 nm or 532 nm excitation. Particle excitation by 354 nm at energies >0.5 mJ created a long time (>0.1 s) perturbation of the discharge chemistry which linearly increased the steady state (10 Hz) light scattering with increasing 354 nm energy.

[a]To whom correspondence should be addressed.

[b]Currently at Amoco Corporation, Corporate Research. P.O. Box 400, Naperville, IL 60566.

INTRODUCTION

Parallel plate rf discharges are becoming widely used in the electronics industry for etching and deposition of semiconductor materials. In order to optimize these processes, one needs to understand the complicated chemical and physical processes that occur in the discharge. In this paper we will review our previous results (1-4) and present new data from experiments in which a laser probe is used to investigate the gas phase processes that occur in an rf glow discharge of silane and argon. These discharges are used to produce thin films of photosensitive hydrogenated amorphous silicon, which have been applied in photovoltaic devices, electrophotography processes and thin film transistors (5).

When describing the gas phase processes that occur in rf discharges one can speak of two basic regions: the plasma and the sheaths. A plasma, as defined by Langmuir (6), is a partially ionized gas in which the Debye length is small compared to other macroscopic lengths. This implies that a plasma contains an equal number of positive ions and negatively charged electrons and anions. In rf discharges one generally describes the central region that emits visible radiation as the plasma region. The sheath region is a transition zone from the plasma to an electrode which serves to maintain equal flux at the electrodes between the highly mobile electrons and the much slower cations. These sheath regions are generally dark spaces due to low electron densities and have time dependent as well as average properties in an rf discharge. Recently there have been a number of experimental measurements (7-11) and theoretical calculations (12-14) that have provided insights into the microscopic and macroscopic behavior of rf discharge sheaths.

The nature of the interface between the space charge in the sheath region and the neutral plasma is difficult to define even in well understood dc discharges (15). In rf discharges the possible complexity of this interface region increases due to the time dependent nature of both the fields in the sheath and the position of the sheath edge. When one considers the chemistry that is involved, the problem gets more complex and anticipating any given phenomenon is difficult. In our experiments with laser probes we have identified phenomena in discharges of silane and argon that are difficult to explain in terms of simple models of the rf discharge (16). We have found that unusual chemistry can occur in rf discharges in very sharply defined regions associated with the sheath-plasma interface.

EXPERIMENTAL

The vacuum chamber was a 76.2 mm inside diameter stainless steel cross which was modified by adding two windows mounted perpendicular to the plane of the cross and displaced from the cross center by 12.5 cm. The windows were mounted at Brewster's angle to minimize scattered light from the lasers. The cross was parallel to the table and plane parallel electrodes were inserted in two opposing ports of the cross to define a discharge region viewable from a perpendicular port. Figure 1 shows the top view of the cross with the flexible pumping port and monochromator viewing window. The viewing window was further displaced from the discharge region to define a larger length for gas flow stabilization and minimization of window contamination by plasma products. The laser beam entered and exited perpendicular to the

plane of the cross. The focal point of the beam was on the center line of the two electrodes and it was imaged on the vertical slit of a monochromator. The vacuum chamber was mounted on a set of stages which could be translated in reference to the fixed laser beam to obtain spatial profiles. The length of the spatial scan depended on the orientation of the Brewster windows, which was determined by the polarization of the laser beam. For a beam that was linearly polarized in the plane defined by the laser beam and the monochromator slit, the maximum scan was 25 mm. For a beam polarized perpendicular to this plane, as was needed for optimized light scattering, the maximum scan was 12 mm. In the latter window geometry, the electrodes must be repositioned to study the discharge at both electrodes. The pressure in the chamber was measured with a capacitive manometer. The powered electrode was 38 mm in diameter and the ground electrode was 50.8 mm diameter. The powered electrode was isolated from the discharge chamber while the other electrode was in mutual ground with the chamber. Attached to the grounded electrode was a screen of 68.6 mm diameter that contained the discharge and thus prevented rapid film deposition on the chamber windows. The screen had a square mesh of 4.7/cm with 1.5 mm openings and slotted openings were present to allow complete spatial scans by the laser. The monochromator viewing window imaged the discharge through a screen section in which all wires parallel to the laser were removed to prevent spatially varying collection efficiency. The areas of the two electrodes were nearly the same, however the effective area of the grounded surface in contact with the discharge was much larger than the area of the powered electrode. This caused a negative bias to develop on the powered electrode.

The gas supply used in these experiments was either a 10% or a 0.5% silane in argon mixture provided by Matheson Gas Company. These gas mixtures were further diluted with pure argon in a gas handling manifold. The silane mixture gas flow was controlled with a mass flow controller and the argon diluent with a precision needle valve. The 3.8 cm diameter flexible pumping port was connected to a large, multibaffled trap composed of a series of 15 cm diameter plates. This trap collected particles formed in the discharge before they reached a 15 cfm mechanical vacuum pump. A servo controlled argon leak and a large valve were interposed between the trap and vacuum pump. This allowed precision, long term control of the chamber pressure over a wide range of values without back diffusion into the chamber. The servo valve was referenced to the chamber pressure readout, which allowed pressure stability of 0.001 torr. At 50 sccm, the initial chamber pressure of ~0.16 torr could be set to pressures as large as 0.6 torr by the argon flow adjustment, while larger pressures required the manual valve. The second stage of the pump had a steady flow of nitrogen, and the exhaust from the pump passed through an oven heated to 700°C to decompose the unreacted silane. The oven effluent was vented through a dual-chamber bubbler, containing water, to the lab exhaust system.

Our laser system was a Quanta Ray PDL-1 dye laser pumped by a pulsed Nd:YAG laser (Quanta Ray DCR-1). The dye beam could be frequency doubled to produce a tunable UV beam. The dye laser was operated at 10 Hz and produced light pulses that were 5 ns in duration with energies of a few millijoules in the visible, and a few tenths of millijoules in the UV. The harmonics of a second Quanta Ray Nd:YAG laser were used as a pump beam in two laser pump-probe experiments. The laser beam was focused through the Brewster windows

into the chamber by a telescope quartz lens pair. The image size at focus was 0.1-0.2 mm in diameter as determined from film burn patterns. The signal induced by the laser was detected at a 90° angle through a symmetric quartz lens pair. The laser beam was imaged onto the slit of a 0.75 m monochromator with an f8 collection efficiency from the discharge. The signal from the exit slit of the monochromator was detected on a photomultiplier tube. A fast, gated integration (Lecroy 2249W) of 100 ns provided digital signals to a microcomputer through a CAMAC interface controlled by the Lecroy 8901 IEEE 488 bus converter. A Commodore microcomputer controlled the entire experiment, which allowed efficient data collection and signal averaging. The monochromator, the 5 ns pulse length, and the gated detection all served to discriminate against plasma emission. Photodiode channels were used to monitor laser intensity.

The apparatus was calibrated by filling the chamber with 0.10 torr of benzene vapor and exciting the well known fluorescence spectrum (17). Spatial scans of the benzene fluorescence signal showed a smooth and linear profile that increased slightly, about 5%, from the cathode to the anode. This increase was an experimental artifact and has not been normalized in the measured signals since the measured signals have much larger spatial variations. Absolute quantum yields for benzene fluorescence (18) have been obtained for the calibration transition. This allows us to determine absolute concentration of any species that has a known fluorescent yield.

The range of the discharge parameters we have studied are given in Table 1. The details of the experiments we have performed are given below:

(1) Silicon atom fluorescence was created by focusing the UV laser beam into the discharge region. The laser wavelength of 251.43 nm excites ground state Si, $3p^2\ ^3P_0 \rightarrow 4s\ ^3P_1^o$, and the fluorescence transition $4s\ ^3P_1^o \rightarrow 3p^2\ ^3P_2$ at 252.85 nm was detected through the monochromator. The monochromator resolution of 0.5 nm cleanly separates the 252.85 nm emission from the excitation line and other members of the triplet emission. The polarization chosen for these experiments minimized light scattering and provided spatial scans of the full 22 mm electrode separation.

(2) Light scattering from particles was initially investigated using a laser beam tuned to 500 nm. There was no a priori reason for choosing this wavelength. The polarization for these experiments maximized the scattering signal. Scans of about half the electrode separation could be obtained with this polarization.

(3) Light scattering and fluorescence were determined sequentially by using 251.43 nm excitation with the polarization for maximum scattering. The intensity of the scattering signal in this configuration was 20-25 times greater than the fluorescence signal at 252.85 nm. The resolution of the monochromator allowed the fluorescence signal to be studied without interference from the light scattering signal.

(4) A two laser pump-probe experiment was used to investigate the silicon atom fluorescence signal. The pump laser beam was operated at three of the harmonic wavelengths of the Nd:YAG laser: 532 nm, 354 nm, and 266 nm. The probe beam was operated at 251.43. The two beams were focused colinearly into the discharge and the energy and the triggering of the lasers were controlled independently. This allowed the nonresonant pump beam energy to be varied while maintaining the resonant probe beam at a fixed energy. The

probe beam was inserted at variable times before and after the pump beam. Our pump laser could be triggered up to 300 ns prior to the probe laser and delayed 75 nsec after the probe laser. The triggering time jitter was approximately ±25 ns and laser power was directly measured with a calorimeter at larger energies. Wedged beam splitters and a photodiode were used for extrapolation to low pulse energies. Colinearity was achieved by reflecting the pump laser from a wedged quartz plate or dichroic mirror placed in the path of the probe laser. A second lens pair was used to adjust the pump laser divergence prior to the beam combining optic.

(5) Laser excitation and time resolved emission was done by pumping with 354 nm and 266 nm laser pulses while observing the emission through a monochromator. The emission detection electronics used a time-delayed gate to map a time decay profile. A survey scan was done from 650 nm to 230 nm to identify strong emission lines during a 1 microsecond gate. Time scans at specific wavelengths used 25 and 100 ns gate widths.

REVIEW OF PREVIOUS WORK

The original goal of previous experiments was to detect spatial variations of radical species in silane glow discharges with laser fluorescence and other laser spectroscopic techniques. This study of gas phase chemistry in glow discharge depositions has yet to be completed, although the early results have clearly identified a number of unexpected phenomena. The primary new observation was the existence of spatially well defined zones of particles, even at low silane mole fractions. A short summary of the earlier work is essential to introduce our experimental charac-

terization of particle phenomena at low mole fractions of silane and our new studies of high power laser effects on particles.

The first experiments (1) explored laser excitation and fluorescence detection of ground state silicon atoms as a function of spatial position. These atom fluorescence signals revealed a sharp reduction in fluorescence near the expected ion sheath location. The use of pulsed laser light scattering (2) revealed a large, spatially narrow peak in light scattering intensity near each sheath. In addition, these light scattering profiles showed substructure and spatial features dependent on the pressure, mole fraction of silane, and gas flow. The pressure effect in both silicon-fluorescence and light scattering showed good correlation with models of ion sheaths that predict a constant product of pressure and displacement from the electrode (19). The light scattering increased as the silane mole fraction decreased from 8-2%. This behavior is probably related to the changes in the discharge created by silane, and research is in progress to develop a microscopic model of the relation between particle growth and microscopic changes in discharge chemistry (16). The scattering at 5% silane showed a logarithmic increase with decreasing flow rate (3), an effect expected if particle growth is correlated to residence time in the plasma.

The sharp spatial features in the atom fluorescence signals as well as the light scattering signals suggested that silicon atoms could be formed by laser interaction with particles. This hypothesis was supported by our observation (4) of a non-linear power dependence of the Si fluorescence, which implied that a multiphoton process could be creating atoms during the 5 ns laser pulse at 251.43 nm. Furthermore, a correlation between the atom signals and light scattering signals seemed justified because both signals

increased with decreasing silane mole fraction over the 2-8% range and showed similar displacements in spatial location with pressure changes.

In order to further characterize the relation between atoms and particles we subsequently performed a series of measurements at silane mole fractions ranging from 0.45% to 0.05%. These low mole fractions approximate an argon discharge with weak perturbation by silane (3,4). A useful comparative experiment was the alternate detection of Si fluorescence and light scattering with 251.43 nm excitation. Figure 2 shows that both particle light scattering and atom fluorescence have similar spatial profiles (3,4). This type of spatial tracking to positions near the middle of the discharge suggests a particle precursor for the laser formation of atoms. A radical precursor is not a likely source of atoms because one expects the zone between the sheaths to be uniform in radical concentration for the observed range of silane.

NEW RESULTS

The general goals of this work were to characterize laser-particle interactions and the spatial profiles of particles in discharges which have low mole fractions of silane.

The laser-particle interactions are intrinsically interesting examples of photophysics as well as possible sources of artifacts in laser diagnostics of molecular species in discharges. A specific goal of this study was to confirm that silicon atoms are formed from particle interaction with ultraviolet lasers and to examine the population of silicon excited states. A second goal was to measure atom formation at several wavelengths and to use

light scattering to probe for high energy laser effects on particle growth, nucleation, and fragmentation.

The spatial characterization of particle light scattering was done to explore the range of particle nucleation and growth accessible to light scattering techniques. We specifically compared both electrodes as a function of mole fraction and flow rates of silane. In addition, we compared ultraviolet and visible wavelengths as a function of spatial position in order to identify particle specific wavelength effects.

Laser Interactions with Particles

In order to probe atom formation mechanisms we used two independent lasers at a colinear focus in the two laser pump-probe geometry described earlier. The probe laser was of constant energy at 251.43 nm and we varied the energy of 266 nm under conditions of pulse coincidence. This extended our previous study of atom formation to much larger pulse energies. Figure 3 shows the data for this laser arrangement at a silane mole fraction of 0.45% and a spatial location of 3.75 mm from the grounded electrode. The emission signal obtained with 266 nm alone is essentially our background, while the 251.4 excitation caused atom fluorescence at a constant value. The use of both 251.4 and 266 nm excitation clearly shows a nearly linear increase of atom fluorescence with increasing energy of 266 nm light. In Figure 4 we show the atom fluorescence signal as a function of probe (251.43 nm) time delay with respect to 266 nm laser excitation at a fixed energy of 0.5 mJ. There is a slight increase in fluorescence as the time delay decreases, and the signal suddenly reduces to the baseline value of the probe when the 266 nm pulse enters after the probe pulse. Atom diffusion out of the focal volume is compatible with the atom fluorescence reduction at long probe

delays. The sudden reduction in signal shown in Figure 4 implies that atoms are formed from each laser pulse rather than from cumulative effects of our 10 Hz laser excitation.

The 266 nm pulse clearly is responsible for atom creation from some species that we have associated with particles, although not necessarily the same particles that dominate the light scattering. We monitored the light scattering of 251.43 nm as a function of 266 nm power and time delay, and we found no dependence of light scattering intensity on 266 nm power with 0.45% silane discharges over the complete spatial profile. This result shows that 266 nm (or 251.43 nm) excitation creates atoms without significantly affecting the particle distribution monitored by light scattering at 251.43 nm. The light scattering signal is a convolution of size and number density, which implies that atoms might be generated photochemically from local areas of the dominant sized particle species or from smaller species. Resonant absorption effects could be important in defining photochemical interactions leading to atoms and radicals.

Results in Figure 5 show that 266 nm excitation creates intense emission at 288.16 nm from silicon atoms in their $4s\ ^1P_1^o$ state emitting to the $3p^2\ ^1D_2$ state that is 0.78 eV above the ground state. The emission was very intense during the laser pulse and progressively decreased in time. The 288.16 nm emission (and emission from the same state at 390.59 nm) at long times (>450 ns) after the laser pulse is due to electron impact excitation of metastable silicon in the $3p^2\ ^1D_2$ state, although under the same conditions there was negligible emission at 251.4 nm from excited ($^3P_1^o$) ground state silicon atoms. It is important that in the absence of the laser, there was

negligible emisson detected from the normal plasma process that emits at 288.16 nm. This is because of the short gate times in the experiment. Future experiments will normalize the wavelength sensitivity of the apparatus and use laser excitation to determine the relative state population of silicon atoms. We also will search for other radical species created by 266 nm excitation.

The preceding experiments with 266 nm excitation were extended to excitation with 354 nm and 532 nm. Simultaneous with excitation by 354 nm and 532 nm we monitored Si atom fluorescence and light scattering by 251.4 nm excitation. The 532 nm excitation, at energies up to 9 mJ, showed no changes in atom concentration or 251.4 nm light scattering intensity for silane mole fractions of 0.45%. With 354 nm excitation there was no creation of atom fluorescence at energies up to 2 mJ, but an unusual change in light scattering occurred at this wavelength. Figure 6 shows the variation of light scattering signal from 251.43 nm when the 354 nm pump beam was coincident. A time delay experiment similar to Fig. 4 established that the increase in light scatter is a long time effect arising from the <u>preceding</u> laser pulses in the 10 Hz excitation. These two results show that 354 nm excitation is not capable of creating silicon atoms by photodecomposition processes, but it is capable of creating sufficient fragmentation or radical interaction to change the particle size or number density a large amount. Experiments monitoring the time resolved emission following 354 nm excitation identified no emission features, a result compatible with no observation of silicon atoms. Further studies of wavelength effects are in progress to understand the nature of laser-particle interactions in these discharges.

In summary, laser interactions with particles in a silane discharge show a number of unusual wavelength dependent effects. Ultraviolet pulsed lasers of 251.4 nm or 266 nm formed ground state silicon atoms from particles with a nearly linear increase in atom concentration with increasing laser energy. Silicon atom emission was also observed from metastable singlet states of silicon atoms after their formation by 266 nm pulses but not from excited triplet states. However, no atoms were created with 354 nm or 532 nm excitation. Neither ultraviolet excitation nor 532 nm excitation affected the intensity or spatial profile of ultraviolet light scattering. However, 354 nm excitation strongly perturbed the discharge chemistry over long time scales of >0.1 s. This perturbation caused an increase in 251.4 nm light scattering with increased energy at 354 nm. This effect was a result of additional particle nucleation or growth.

<u>Particle Distributions</u>

Spatial scans of laser light scattering were done with a number of systematic variations of macroscopic rf discharge parameters similar to our earlier work (2,3) at larger mole fractions of silane. We have completed scans near both electrodes in <u>separate</u> experiments. As explained in the experimental section, the required modification of electrode position in the chamber can slightly alter the discharge characteristics. This means that light scattering signals are not directly comparable for both electrodes. In addition, very subtle changes in particle nucleation and growth can be sensitive to these apparatus variations. Consequently, systematic changes are best analyzed for each electrode separately until an improved apparatus allows full spatial scans.

The results in Figure 7 show spatial distributions of light scattering that we obtained with 10 ns pulses of 532 nm radiation at 0.05 mJ/pulse. We compared several scans for laser energies from 0.02-0.15 mJ to confirm that no perturbations were present due to laser power effects. The grounded electrode (at 0 mm) portion of the discharge shows a peak at the region of the ion sheath that progressively increases with decreasing mole fraction until a rather dramatic change in position and shape occurs between 0.25 and 0.2% silane. The 0.15% curve is not shown, but it is similar to the 0.2% curve. A second dramatic change occurs from 0.15% to 0.1% mole fraction where the light scattering was reduced to our background level. The light scattering near the rf electrode (22 mm) shows a narrow spatial peak that increases from 0.45% to 0.3% (not shown). At 0.25% silane a small shift and substantial broadening occurs until the signal disappears at a mole fraction of 0.15%. While we cannot compare both sides of the discharge exactly, it appears that a large drop in signal occurs at both electrodes between 0.1 and 0.15% silane. At slightly larger mole fractions there is a large spatial shift near the ground electrode.

The data in Fig. 7 near the ground electrode are quite different from our previous observations (4) with 251.4 nm light scattering under nearly identical plasma conditions. Several spatial profiles at 251.4 nm are shown in Fig. 2. In these data the peak shape changes at 0.4% silane (not shown) to a sharp edged plateau. A progressive edge movement towards the center of the discharge commences at 0.35% silane. We have done a confirmation of these shape differences by comparing 532 and 266 nm scattering in the same plasma. Although more experiments are in progress to achieve a multiple wavelength scan with very precise colinearity and intensity calibration, the

main conclusion is that each wavelength is probing a different aspect of the particle distribution. Electronic resonance effects could be important in a wavelength dependence of this type, and of course, these effects can also depend on particle size and composition.

The mole fraction variation in light scattering intensity shown in Fig. 7 provides some general trends at both electrodes. The <u>increase</u> in light scattering with <u>decreasing</u> silane mole fraction occurs for 532 nm excitation, until the mole fraction reaches 0.25%. This behavior was also observed for much larger mole fractions and a 500 nm probe laser (2). One qualitative interpretation of this result is that the concentration of silane must reach a very low value before the electron collision dynamics are controlled by the argon, especially at the ion sheath. Such an effect will occur by reducing the amount of silane to a point where its number density and enhanced cross sections for electron interaction are dominated by electron-argon processes. The enhancement of particle scattering by reduction of silane correlates with enhanced nucleation or growth. Both kinetic processes can be increased with more energetic electron distributions through increased silane fragment ionization (nucleation) and radical formation (nucleation and growth). The observation that 266 nm and 532 nm light scattering show widely different spatial trends as a function of mole fraction implies that particles may have compositions that are affected differently by radical and ion formation kinetics.

An experiment that may reveal the roles of nucleation and growth at various mole fractions is the variation of light scattering with silane flow rate at constant mole fraction and pressure. We show such a flow rate con-

parison in Figure 8 for 0.45% silane at 0.5 torr. Both electrodes show a dramatic increase in light scattering, without significant spatial changes, for a decrease in flow rate from 50 sccm to 30 sccm. This behavior was also observed at mole fractions of 2-9% for 500 nm (4). For the 532 nm scattering we conclude that the kinetic conditions of nucleation and growth at 0.45% silane are very sensitive to residence time. A detailed kinetic model is necessary to understand the roles of nucleation, growth and percentage conversion of silane into radicals.

The effect of flow rates on spatial profiles of light scattering at 0.45% silane should be compared to 0.2% silane, where the discharge is more nearly a perturbation of an argon dominated system. Figure 9 shows these results for both electrode regions with 0.2% silane. The ground electrode clearly shows that a reduced flow rate progressively shifts the light scattering profiles closer to the sheath region and increases the scattered light intensity. Unlike Figure 8, these profiles suggest that nucleation and growth is progressing from the interior to the sheath zone as the residence time increases. The scattering at the rf electrode in Fig. 9 shows slight shifts and amplitude changes similar to Fig. 8, except for the surprising reduction of signal at 30 sccm flow. This sudden reduction of signal is not understood, and more experiments are needed with contiguous scans of both electrodes. We can conclude that flow rate changes at a mole fraction of 0.2% are capable of revealing a full range of spatial shifts near the ground electrode. This range of discharge parameters offers sensitive probes of particle nucleation and growth at each electrode. More experiments and models will be needed to evaluate the role of each electrode in particle nucleation.

In summary, the spatial scans of light scattering have demonstrated that the ground electrode region is most sensitive to silane mole fraction changes. Visible and ultraviolet wavelengths are probing different aspects of the particle distribution, as was shown by their different light scattering profiles for changing silane concentrations and flow rates. We observed flow rate variations at 0.45% silane that were quite different from 0.20% and concluded that very low mole fractions may be necessary to reach discharge conditions dominated by argon rather than silane. The sensitivity of the light scattering spatial profiles to small changes in mole fraction of silane and flow indicates that these experiments are very suitable for developing and testing models of nucleation and growth in an rf discharge.

CONCLUSIONS

The photophysics of laser-particle interactions in a silane discharge has the following characteristics. Ultraviolet laser pulses (266 and 251.4 nm) interact with particles to form ground state (triplet) silicon atoms and excited state (singlet) silicon atoms, but not excited triplet atoms. Laser pulses of 354 or 532 nm do not form atoms from particle interactions. Laser pulses of 266, 354 or 532 nm do not effect particle light scattering at 254.1 nm on short time scales, but single 354 nm laser pulses effect the nucleation or growth of particles over long time scales. Laser-particle interactions are clearly dominated by wavelength and power effects in the formation of atoms from particles and the perturbation of discharge chemistry. More detailed study of particle photophysics will be necessary to elucidate these phenomena. The future use of laser diagnostics

in rf discharges will need to consider plasma perturbation effects from laser-particle interactions.

The spatial scans of laser light scattering show that ultraviolet and visible wavelengths are probing different aspects of the particle distributions. The ground electrode in our discharge has particle light scattering profiles that are very sensitive to silane mole fractions and flow rates. Future studies of particle number density and size will be necessary to define the particle nucleation and growth phenomena demonstrated in these spatial scans of light scattering.

ACKNOWLEDGMENT

We thank the Office of Naval Research, Chemistry Division for support of this work. In addition, we note that early aspects of this work benefited from the advice and encouragement of the late Gilbert D. Stein of Northwestern University, Department of Mechanical and Nuclear Engineering.

REFERENCES

1. R. M. Roth, K. G. Spears, and G. Wong, "Spatial concentrations of silicon atoms by laser-induced fluorescence in a silane glow discharge", Appl. Phys. Lett., vol. 45, pp. 28-30, July 1, 1984.

2. R. M. Roth, K. G. Spears, G. D. Stein, and G. Wong, "Spatial dependence of particle light scattering in an rf silane discharge", Appl. Phys. Lett., vol. 46, pp. 253-255, Feb. 1, 1985.

3. K. G. Spears and R. M. Roth, "Spatial resolution of small particles in silane discharges", in Plasma Synthesis and Etching of Electronic Materials, R. P. H. Chang and B. Abeles, eds., Pittsburg, PA: Materials Research Society, 1985, pp. 111-116.

4. R. M. Roth, K. G. Spears, and G. Wong, "Spatial concentrations of silicon atoms in rf discharges of silane", in Plasma Synthesis and Etching of Electronic Materials, R. P. H. Chang and B. Abeles, eds., Pittsburg, PA: Materials Research Society, 1985, pp. 117-123.

5. D. Adler, A. Madan, and M. J. Thompson, eds., Materials Issues in Applications of Amorphous Silicon Technology, Pittsburg, PA: Materials Research Society, 1985.

6. I. Langmuir, "The interaction of electron and positive ion space charges in cathode sheaths", Phys. Rev., vol. 33, pp. 954-989, June, 1929.

7. K. Kohler, J. W. Coburn, D. E. Horne, and E. Kay, "Plasma potentials of 13.56-MHz rf argon glow discharges in a planar system", J. Appl. Phys., vol. 57, pp. 59-66, Jan. 1, 1985.

8. C. A. Moore, G. P. Davis, and R. A. Gottscho, "Sensitive, nonintrusive, in-situ measurement of temporally and spatially resolved plasma electric fields", Phys. Rev. Lett., vol. 52, pp. 538-541, Feb. 13, 1984.

9. R. A. Gottscho, R. H. Burton, D. L. Flamm, V. M. Donnelly, and G. P. Davis, "Ion dynamics of rf plasmas and plasma sheaths: A time-resolved spectroscopic study", J. Appl. Phys., vol. 55, pp. 2707-2714, April 1, 1984.

10. T. D. Mantei, "Substrate biasing for plasma etching", J. Electrochem. Soc., vol. 130, pp. 1958-1959, Sept. 1983.

11. C. M. Horwitz, "Rf sputtering-voltage division between two electrodes", J. Vac. Sci. Technol. A, vol. 1, pp. 60-68, Jan. 1983.

12. M. J. Kushner, "Distribution of Ion Energies Incident on Electrodes in RF Discharges for Plasma Processing", to be published, J. Applied Physics.

13. R. A. Gottscho, "Time resolved diagnostics of rf plasmas: A fluid model for ion concentrations in the sheath", in Plasma Synthesis and Etching of Electronic Materials, R. P. H. Chang and B. Abeles, eds., Pittsburg, PA: Materials Research Society, 1985, pp. 55-67.

14. M. J. Kushner, W. M. Anderson, and P. J. Hargis, "Simulation of spatially dependent excitation rates and power deposition in rf discharges for plasma processing", in Plasma Synthesis and Etching of Electronic Materials, R. P. H. Chang and B. Abeles, eds., Pittsburg, PA: Materials Research Society, 1985, pp. 201-213.

15. B. N. Chapman, Glow Discharge Processes, New York, NY: John Wiley and Sons, 1980, pp. 65-70.

16. M. J. Kushner, "Mechanisms for Power Deposition in Ar/SiH_4 Capacitively Coupled RF Discharges", see this journal issue.

17. C. S. Parmenter, "Radiative and non-radiative processes in benzene", Adv. Chem. Phys., vol. 22, pp. 365-421, 1972.

18. C. S. Parmenter and M. W. Schuyler, "Single vibronic level fluorescence III. Fluorescence yields from three vibronic levels in the $^1B_{2u}$ state of benzene", Chem. Phys. Lett., vol. 6, pp. 339-341, Aug. 15, 1970.

19. W. B. Pennebaker, "Influence of scattering and ionization on rf impedance in glow discharge sheaths", IBM J. Res. Develop., vol. 23, pp. 16-23, Jan. 1979.

Table I. Ranges of Discharge Operating Parameters Investigated in the Experiments.

Electrode spacing	22 mm
Substrate temperature	30 C
rf Power	2-5 W
rf Frequency	12 MHz
Negative dc bias	20-200 V
Silane in argon	0.05-9%
Gas flow	20-50 sccm
Gas pressure	0.3-0.9 torr

FIGURE CAPTIONS

Figure 1. Schematic cross section of the discharge chamber (top view). Lasers enter perpendicular to the paper in this view.

Figure 2. Laser light scattering and silicon atom fluorescence for 251.4 nm excitation at various positions in the discharge. The ground electrode is at 0 mm, the pressure is 0.5 Torr, silane-argon mixtures are at 50 sccm flow and the rf power is 3 W. The light scattering for 0.05% silane was negligible and is not shown in panel b.

Figure 3. Silicon atom fluorescence excited by constant energy pulses of 251.4 nm with and without a coaxial and time coincident pulse of 266 nm. Discharge conditions are the same as Fig. 2 with 0.45% silane and a position of 3.75 mm. A control experiment with 266 nm is plotted. The dash line represents the incremental effect of silicon atom formation by 266 nm and the solid line gives a unit slope comparison.

Figure 4. Silicon atom fluorescence excited by a 251.4 nm probe at various delay times following a 266 nm pump pulse of 0.5 mJ. Discharge conditions are the same as Fig. 3 and the time jitter is ±25 ns.

Figure 5. Emission intensity at 288.1 nm from excited silicon atoms formed by 266 nm excitation at 0.5 mJ. Discharge conditions are the same as Fig. 3 and the integration gate width was increased to 100 ns after 150 nsec delay. Gate centers are plotted on the time axis.

Figure 6. Light scattering from 251.4 nm, with and without a coaxial and time coincident pulse of 354 nm. Discharge conditions are the same as Figure 3 with a 10 Hz laser excitation. A control experiment with 354 nm is plotted.

Figure 7. Light scattering from 532 nm as a function of position in the discharge. Discharge conditions are the same as Figure 2 and the mole fraction is varied. The ground electrode (0 mm) and rf electrode (22 mm) experiments are in two separate geometries. A plot of 0.15% (not shown) silane is similar to the 0.20% case in panel a. In panel b the 0.15% case is similar to the 0.10% scan that shows negligible scattering.

Figure 8. Light scattering from 532 nm as a function of gas flow at 0.45% silane in argon. Discharge conditions are the same as Fig. 2.

Figure 9. Light scattering from 532 nm as a function of gas flow at 0.20% silane in argon. Discharge conditions are the same as Fig. 2. No scatter is observed in panel b for 20 or 30 sccm.

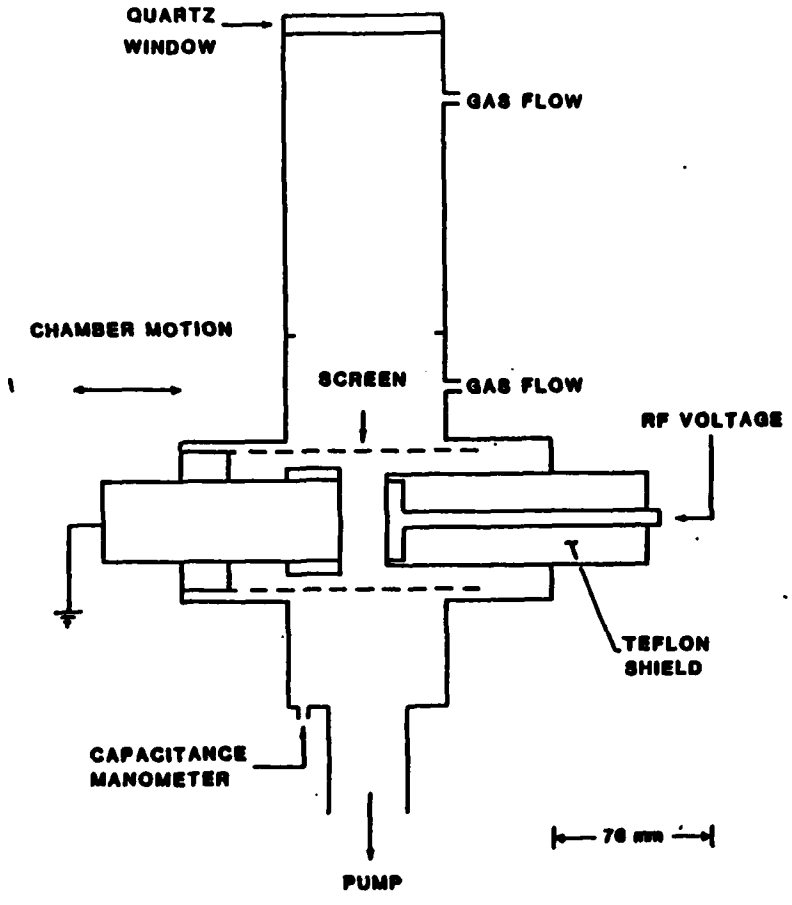
QUARTZ
WINDOW
GAS FLOW
CHAMBER MOTION
SCREEN
GAS FLOW
RF VOLTAGE
TEFLON
SHIELD
CAPACITANCE
MANOMETER
76 mm
PUMP

FIG 1

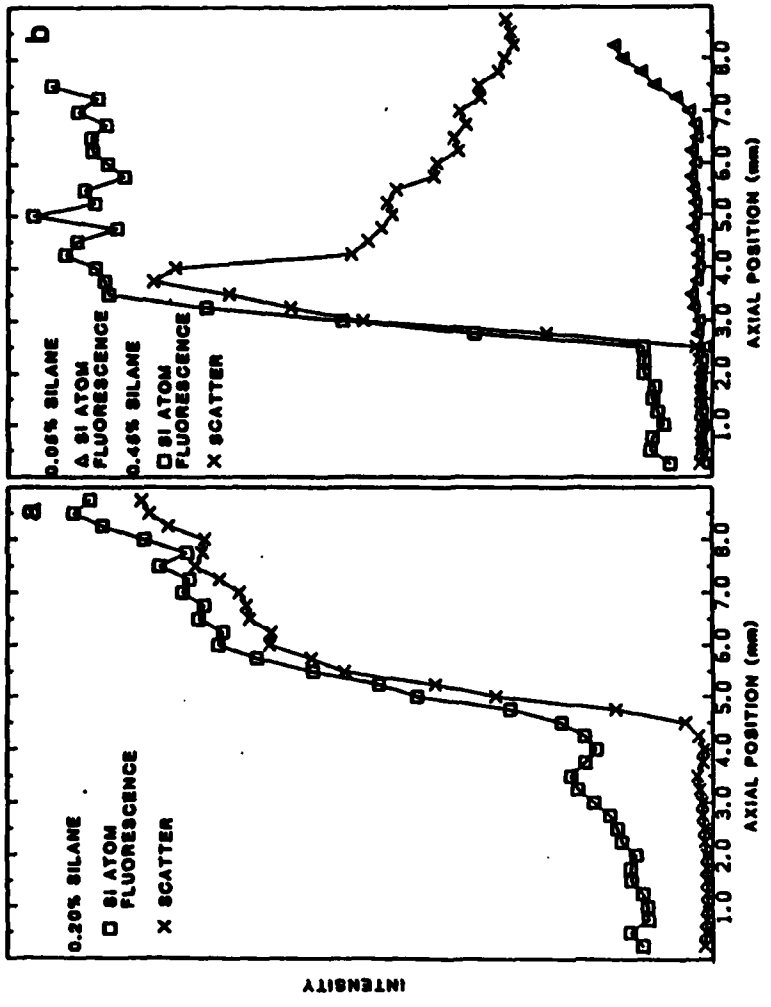
b
0.05% SILANE
Δ SI ATOM FLUORESCENCE
0.46% SILANE
□ SI ATOM FLUORESCENCE
× SCATTER
a
0.20% SILANE
□ SI ATOM FLUORESCENCE
× SCATTER
1.0 2.0 3.0 4.0 5.0 6.0 7.0 8.0
AXIAL POSITION (mm)
INTENSITY

FIG 2

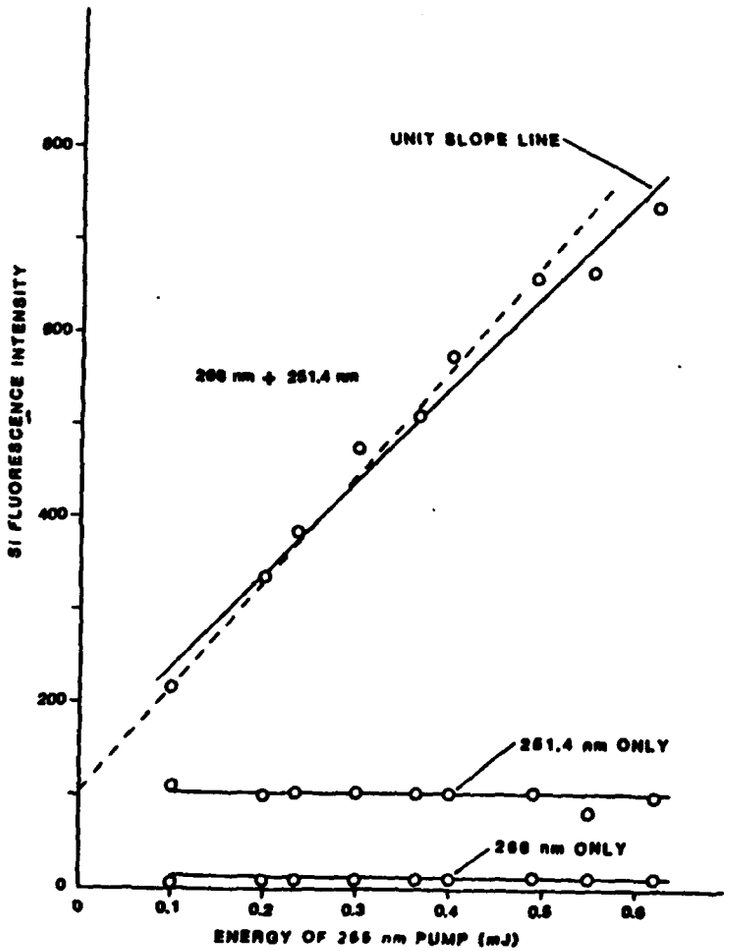
UNIT SLOPE LINE
266 nm + 251.4 nm
251.4 nm ONLY
266 nm ONLY
SI FLUORESCENCE INTENSITY
ENERGY OF 266 nm PUMP (mJ)
0
200
400
600
0.1
0.2
0.3
0.4
0.5
0.6

FIG 3

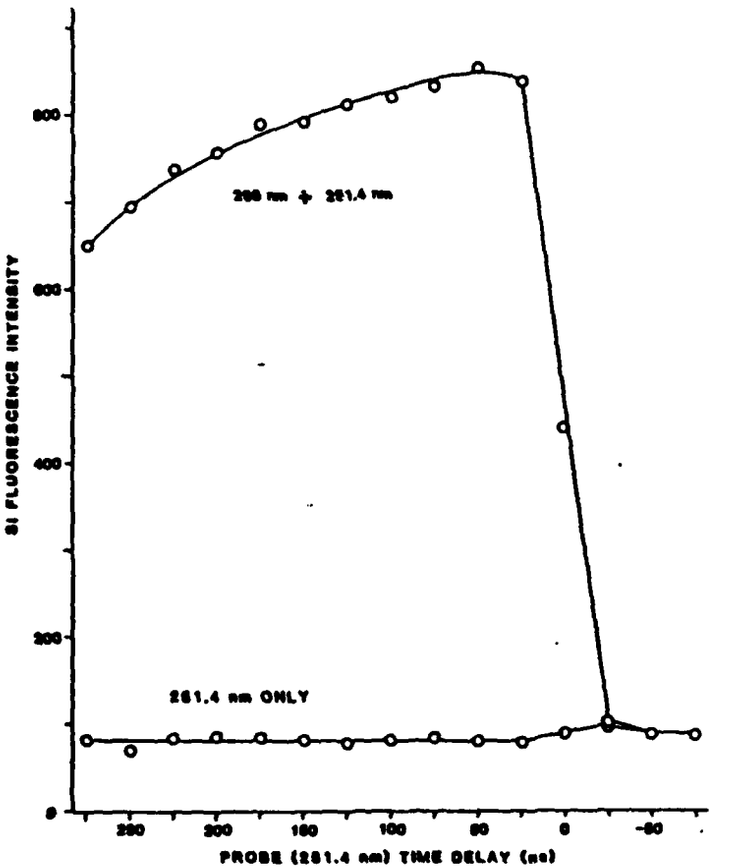
266 nm + 251.4 nm
251.4 nm ONLY
SI FLUORESCENCE INTENSITY
PROBE (251.4 nm) TIME DELAY (ns)
0
200
400
600
250
200
150
100
50
0
-50

FIG 4

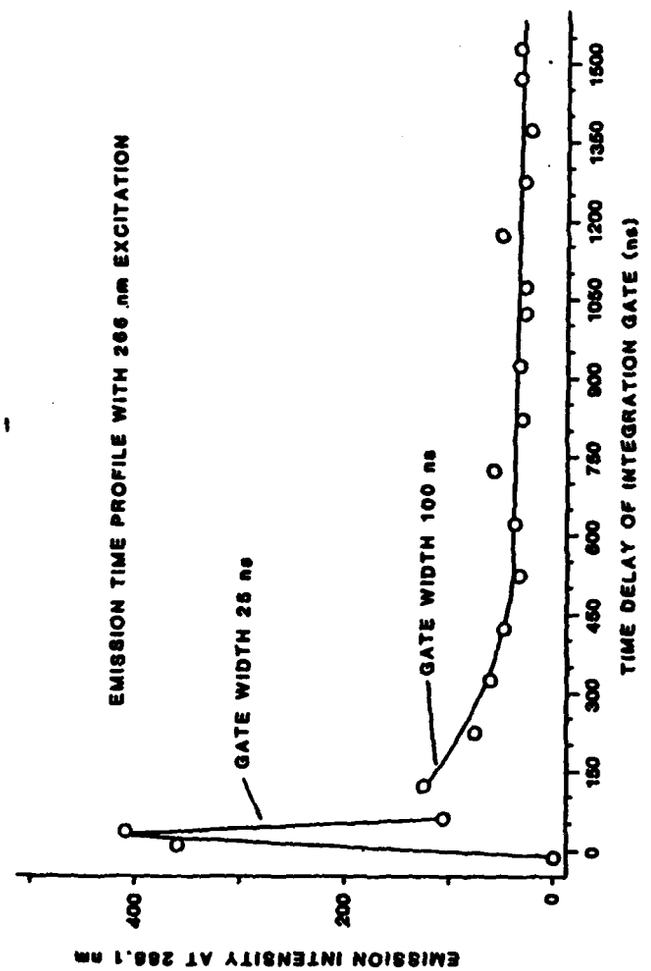
EMISSION TIME PROFILE WITH 266 nm EXCITATION
GATE WIDTH 25 ns
GATE WIDTH 100 ns
TIME DELAY OF INTEGRATION GATE (ns)
EMISSION INTENSITY AT 288.1 nm
0
150
300
450
600
750
800
1050
1200
1350
1500
400
200
0

F165

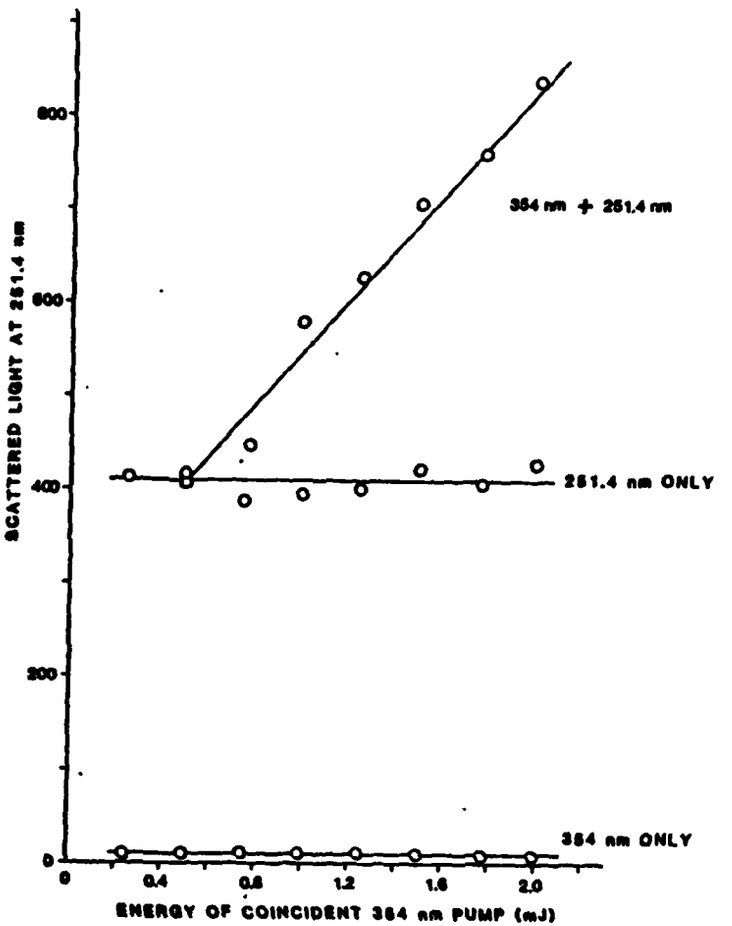
SCATTERED LIGHT AT 251.4 nm
800
600
400
200
0
354 nm + 251.4 nm
251.4 nm ONLY
354 nm ONLY
0
0.4
0.8
1.2
1.6
2.0
ENERGY OF COINCIDENT 354 nm PUMP (mJ)

F166

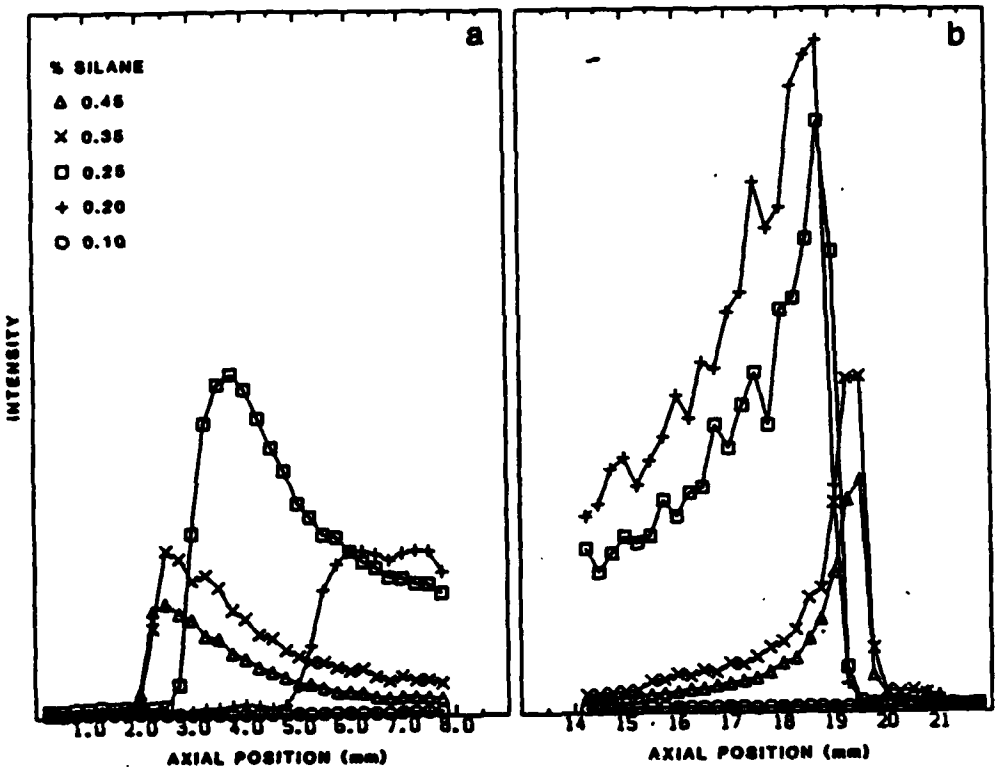
a
b
% SILANE
0.45
0.35
0.25
0.20
0.10
INTENSITY
1.0 2.0 3.0 4.0 5.0 6.0 7.0 8.0
AXIAL POSITION (mm)
14 15 16 17 18 19 20 21
AXIAL POSITION (mm)

FIG 7

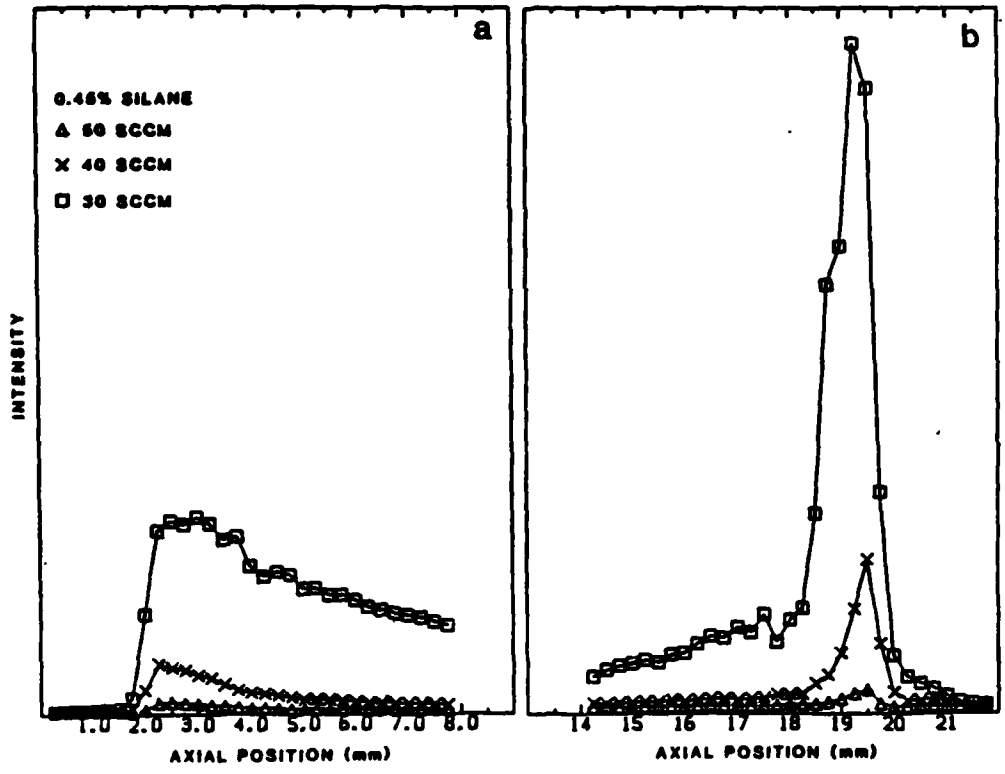
a
b
0.45% SILANE
50 SCCM
40 SCCM
30 SCCM
INTENSITY
1.0 2.0 3.0 4.0 5.0 6.0 7.0 8.0
AXIAL POSITION (mm)
14 15 16 17 18 19 20 21
AXIAL POSITION (mm)

FIG 8

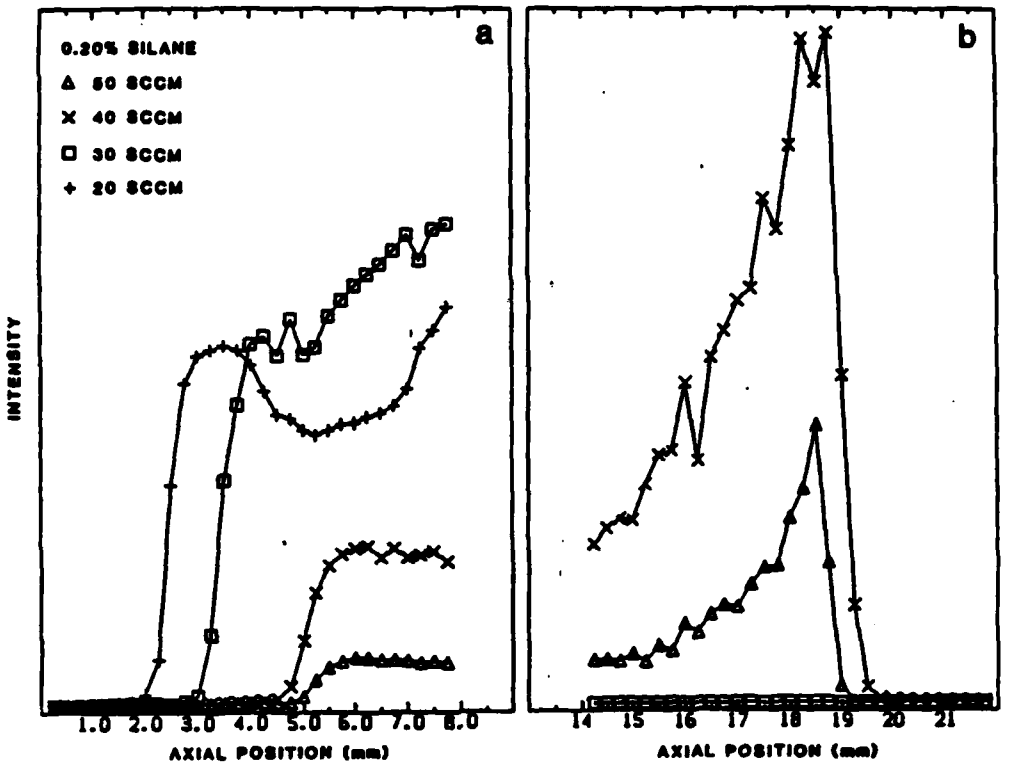
0.20% SILANE
Δ 50 SCCM
× 40 SCCM
□ 30 SCCM
+ 20 SCCM
a
b
INTENSITY
1.0 2.0 3.0 4.0 5.0 6.0 7.0 8.0
AXIAL POSITION (mm)
14 15 16 17 18 19 20 21
AXIAL POSITION (mm)

Fig-9

END

FILMED

1-86

DTIC